arXiv:astro-ph/0701273v1 9 Jan 2007

STUDYING THE EVOLUTION OF LARGE-SCALE STRUCTURE WITH THE VIMOS-VLT DEEP SURVEY

LUIGI GUZZO[1,2] and the VVDS Consortium*
[1] *INAF - Osservatorio Astronomico di Brera, Milan, Italy*

The VIMOS-VLT Deep Survey (VVDS) currently offers a unique combination of depth, angular size and number of measured galaxies among surveys of the distant Universe: $\sim 11,000$ spectra over 0.5 deg^2 to $I_{AB} = 24$ (*VVDS-Deep*), $35,000$ spectra over ~ 7 deg^2 to $I_{AB} = 22.5$ (*VVDS-Wide*). The current "First Epoch" data from VVDS-Deep already allow investigations of galaxy clustering and its dependence on galaxy properties to be extended to redshifts $\sim 1.2 - 1.5$, in addition to measuring accurately evolution in the properties of galaxies up to $z \sim 4$. This paper concentrates on the main results obtained so far on galaxy clustering. L_B^* galaxies at $z \simeq 1.5$ show a correlation length $r_0 = 3.6 \pm 0.7$. As a consequence, the linear galaxy bias at fixed luminosity rises over the same range from the value $b_L \simeq 1$ measured locally, to $b_L = 1.5 \pm 0.1$. The interplay of galaxy and structure evolution in producing this observation is discussed in some detail. Galaxy clustering is found to depend on galaxy luminosity also at $z \simeq 1$, but luminous galaxies at this redshift show a significantly steeper small-scale correlation function than their $z = 0$ counterparts. Finally, red galaxies remain more clustered than blue galaxies out to similar redshifts, with a nearly constant relative bias among the two classes, $b_{rel} \simeq 1.4$, despite the rather dramatic evolution in the color-density relation over the same redshift range.

1 Introduction

During the last few years, our knowledge of the large-scale structure of the Universe has reached an exquisite level of accuracy. This has been the result of extensive surveys of galaxy redshifts, as

[2] *Visiting Scientist, European Southern Observatory & Max-Planck Gesellschaft, Garching, D*

* *The VVDS Consortium:* O. Le Fèvre (LAM Marseille), G. Vettolani (INAF-IRA Bologna), C. Adami (LAM Marseille), S. Arnouts (LAM Marseille), S. Bardelli (INAF-OA Bologna), M. Bolzonella (INAF-OA Bologna), M. Bondi (INAF-IRA Bologna), A. Bongiorno (Univ. Bologna), D. Bottini (INAF-IASF Milano), J. Brinchmann (Porto), A. Cappi (INAF-OA Bologna), S. Charlot (IAP Paris), P. Ciliegi (INAF-OA Bologna), T. Contini (Toulouse), O. Cucciati (INAF-OA Brera), S. De la Torre (LAM Marseille), S. Foucaud (Nottingham), P. Franzetti (INAF-IASF Milano), B. Garilli (INAF-IASF Milano), I. Gavignaud (AIP Potsdam), L. Guzzo (INAF-OA Brera), O. Ilbert (IfA Hawaii), A. Iovino (INAF-OA Brera), F. Lamareille (INAF-OA Bologna), V. Le Brun (LAM Marseille), D. Maccagni (INAF-IASF Milano), H.J. McCracken (IAP Paris), B. Marano (Univ. Bologna), C. Marinoni (Univ. Marseille), A. Mazure (LAM Marseille), Y. Mellier (IAP Paris), B. Meneux (INAF Milano), R. Merighi (INAF-OA Bologna), P. Merluzzi (INAF-OA Napoli), S. Paltani (ISDC Geneva), R. Pellò (Toulouse), J.P. Picat (Toulouse), A. Pollo (LAM Marseille & Cracow), L. Pozzetti (INAF-OA Bologna), M. Radovich (INAF-OA Napoli), R. Scaramella (INAF-OA Roma), M. Scodeggio (INAF-IASF Milano), S. Temporin (INAF-OA Brera), L. Tresse (LAM Marseille), D. Vergani (INAF-IASF Milano), C.J. Walcher (LAM Marseille) G. Zamorani (INAF-OA Bologna), A. Zanichelli (INAF-IRA Bologna), E. Zucca (INAF-OA Bologna),

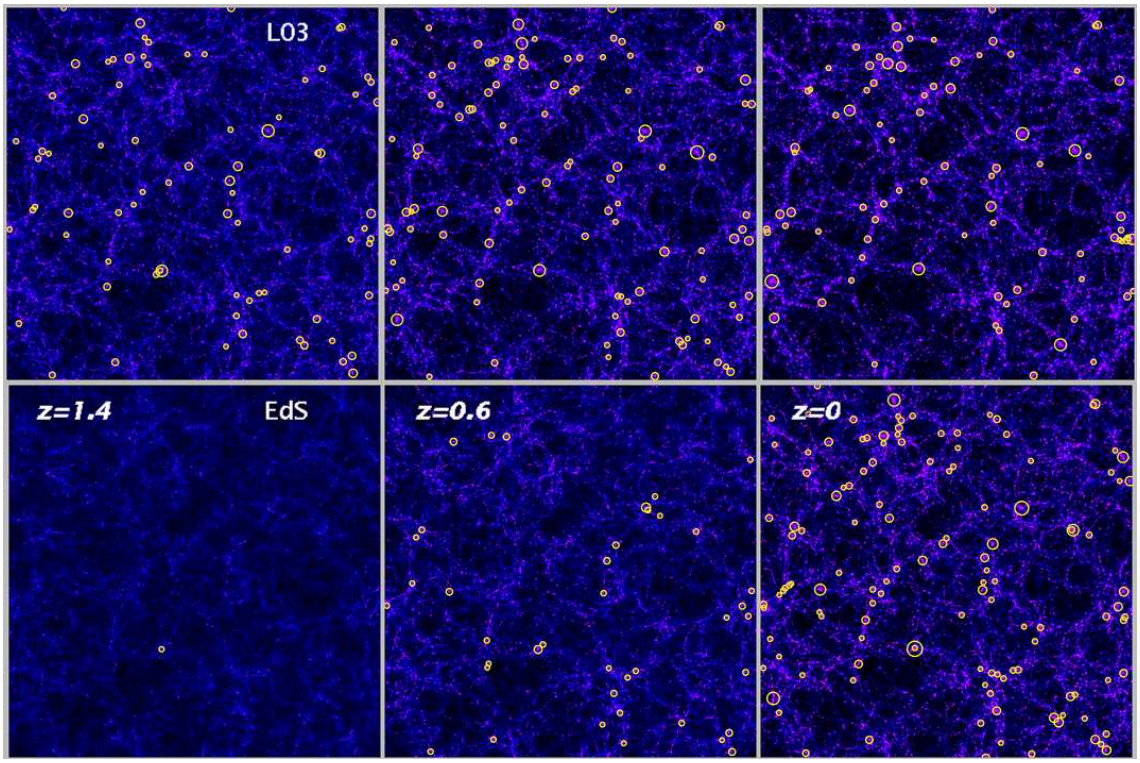

Figure 1: The growth of structure in the Universe simulated through two N-body experiments, both realistic and normalized as to reproduce the observed clustering at the current epoch: a flat low-density model (top, $\Omega_m = 0.3$, $\Omega_\Lambda = 0.7$) and an Einstein–de-Sitter model (bottom, $\Omega_m = 1$). Each of the three redshift snapshots shows a comoving slice of 75 h^{-1} Mpc thicknes and 250 h^{-1} Mpc side. Superimposed on the gray-scale dark matter distribution, circles mark galaxy clusters with masses corresponding to an X–ray temperature $T_X > 3$ keV, with size proportional to T_X (figure from Borgani & Guzzo 2001).

the 2dFGRS (Colless et al. 2001) and SDSS (Adelman-McCarthy et al. 2006), that constructed complete flux-limited samples of several hundred thousand galaxies in the local ($z < 0.2$) Universe, allowing detailed statistical analyses to be performed (e.g. Cole et al. 2005, Eisenstein et al. 2005).

The extension of similar systematic studies of large-scale structure over significant volumes at redshifts approaching unity, is on the other hand relatively recent. Building upon the pioneeristic efforts over very small areas (Broadhurst et al. 1988, Le Fevre et al. 1996, Yee et al. 2000), large ($N > 10,000$) systematic surveys of galaxy redshifts reaching faint flux limits (AB magnitudes fainter than ~ 22.5) and covering *at the same time* areas of the order of or larger than 1 square degree, have become possible only in very recent years, thanks to the construction of highly-multiplexed spectrographs coupled to 8-meter class telescopes. There are currently three such projects ongoing, the VIMOS-VLT Deep Survey, whose clustering results will be the subject of this paper, the DEEP2 survey at Keck (Coil et al. 2006) and the zCOSMOS survey, again using VIMOS at the VLT (Lilly et al. 2007).

Figure 1 shows explicitly which was the main original motivation of astronomers for trying and measure the evolution of galaxy clustering: the way structure grows is a sensitive function of the cosmological model (from Borgani & Guzzo 2001). The top and bottom rows in the figure show snapshots at three different redshifts from two N-body simulations run with different cosmological initial conditions, as described in the caption. Both are normalized as to reproduce the observed clustering at the current epoch. The yellow circles mark the position and mass of galaxy clusters, identified in the simulation as mass concentrations that would shine in X-rays with an equivalent temperature $T_X > 3$ keV. The evolution of large-scale structure with redshift

is dramatically different in the two simulations: in the Einstein-DeSitter model at the bottom (where the flat geometry is provided entirely by matter, $\Omega_M = 1$), a shortage of massive clusters is already observed at redshifts as low as 0.6. On the contrary, the low-Ω_M model shows almost no evolution. The results from deep surveys of X-ray clusters are consistent with this latter picture, showing only a mild decline of the bright end of the cluster X-ray luminosity function for $z > 0.7$ (see Rosati et al. 2002 for a review). Using the evolution of structure sampled via the abundance of clusters at different epochs, therefore, one can obtain fairly robust estimates of the mean density of matter[†], $\Omega_M \simeq 0.3$ (Borgani et al. 2001).

These results from X-ray cluster are made possible by one specific feature: at this level, clusters can be considered as rather simple dark matter halos, for which we have well-calibrated relationships relating the halo total mass and the observed X-ray luminosity. Given a cosmological model and thus a power spectrum of fluctuations, we can robustly predict the number density of DM halos above a given mass at any epoch, via the Press-Schechter (1974) theory and subsequent refinements (e.g. Sheth & Tormen 1999), or via analytic fits to N-body simulations like those of Fig. 1 (e.g. Jenkins et al. 2001). This can then be translated into the expected number of clusters above a given X-ray luminosity, and compared to observations.

The situation with using galaxies as tracers of structure evolution is significantly more complicated: understanding the relationship between dark matter halos and the baryonic component we actually detect in the form of galaxies is in fact one of the major challenges of modern cosmology. Theoretical efforts, in view of the lack of a complete physical descriptions of the large number of nonlinear processes leading to galaxy formation within a dark-matter halo, have necessarily to rely upon a number of well-motivated physical recipes. These are used to describe statistically phenomena like cooling, star formation and heating in the baryonic component, as a function of the properties of the parent halo and, possibly, the surrounding environment. Such semi-analytic scheme is usually applied to the history and distribution of halos (the "merging tree"), obtained via a Montecarlo Press-Schechter approach or from n-body simulations (e.g. Somerville & Primack 1999, Kauffmann et al. 1999, Lacey & Cole 1993). Thus, the effect of the fundamental cosmological parameters that shows up so clearly in the example of Fig. 1, when we come to galaxies is in principle shielded by the myriad of astrophysical processes related to gas and stars.

Nevertheless, the motivation for extensive deep galaxy redshift surveys is not diminished: one wants not only to measure the clustering properties as a function of redshift, but also how these depend, at different cosmic epochs, on physical properties (as e.g. luminosity, star-formation rate, color, morphological type) that are themselves evolving with redshift. The goal becomes thus also understanding how these may be connected, more or less directly, to the mass of the parent halo and/or to the surrounding environment. Changing our initial perspective, therefore, we may say that the main motivation for deep galaxy surveys is not to try and measure cosmological parameters via the growth of DM structure (which is difficult to disentangle from the aforementioned astrophysical effects), but rather learn how galaxies have been forming within DM halos. The hope is that at the end of the day we can close the circle and better understand how to use them to do cosmology[‡].

[†]More precisely, the evolution of the cluster mean density depends both on Ω_M and on the normalization of the power spectrum of fluctuations, traditionally espressed as the *rms* fluctuation in $8\,h^{-1}\,$Mpc spheres, σ_8.

[‡]Throughout the paper we shall use $\Omega_m = 0.3$ and $\Omega_\Lambda = 0.7$, with the Hubble constant usually parameterised via h$= H_0/100$ to ease comparison with previous works; a value $H_0 = 70$ km s^{-1} Mpc^{-1} is used when computing absolute magnitudes.

2 The VIMOS-VLT Deep Survey

The VIMOS-VLT Deep Survey (VVDS) was designed specifically to probe the combined evolution of galaxies and large scale structure to $z \sim 2$ (reaching up to $z \sim 4.5$ with the most extreme objects), by measuring $\sim 100,000$ faint galaxy redshifts. The VVDS is built around the VIMOS multi-object spectrograph at the ESO VLT, capable of simultaneously collecting between 380 and 600 spectra (Le Fèvre et al. 2005). Its source catalogue is selected in the I_{AB} band and the survey is composed by two distinct parts with complementary science goals: *VVDS-Deep*, covering ~ 1 sq. deg. to $I_{AB} = 24$ (5-hour exposures); and *VVDS-Wide*, covering more than 10 sq. deg. to $I_{AB} = 22.5$ (1-hour exposures). Virtually all results presented here are based on the "First Epoch" set of 6530 reliable ($> 80\%$ confidence) redshifts, covering 0.49 square degrees in the "2-hrs field" (F02) of VVDS-Deep. These were collected during the guaranteed-time observations awarded to the Consortium for the construction of VIMOS. The F02 field has also been the subject of extended multi-band observations, including UBVRIK, IR (Spitzer-Swire), radio (VLA) and X-ray (XMM). Another $\sim 33,000$ spectra have already been secured by the *Wide* survey – which is still under completion – and their analysis is undergoing. Details about observations, data reduction, redshift measurement and quality assessment can be found in Le Fèvre et al. (2004; 2005).

3 The evolution of galaxy clustering since $z \sim 1.5$

As with any large redshift survey, the first result from the currently available VVDS data is a cartographic map of the galaxy distribution. The novelty is that the VVDS map is able to cover redshifts never sampled before with similar three-dimensional accuracy. Previous deep surveys were limited to showing peaks and valleys in their 1D redshift histograms, given their small area. With the VVDS, we can for the first time contemplate the appearance of large-scale structure at an epoch when the Universe was about half its current age. An example from a cut-out section of the VVDS "light-cone" between $z = 0.83$ and 0.93 is shown in the left panel of Fig. 2. At this redshift, the survey samples transverse separations of the order of $30\,\mathrm{h}^{-1}\,\mathrm{Mpc}$. Supercluster structures and "voids" similar to those observed by local surveys are clearly emerging. The reader may find this picture somewhat familiar, being used to the similarly beautiful light-cones derived from large numerical simulations. However, while looking at this picture it is worth keeping in mind that this is indeed the real Universe and consider how these maps represent indeed one further step forward in the ever-lasting quest by mankind to explore and chart the surrounding world.

In the following sections, the inhomogeneities that are evident in the galaxy distribution will be quantified in terms of their autocorrelation properties and compared to what we measure at $z \sim 0$.

3.1 Real- and redshift-space correlations at $z \sim 1$

The simplest statistic for studying clustering in the galaxy distribution is the two-point correlation function, $\xi(r)$. This measures the excess probability over random of finding a pair of galaxies with separation r. Since in redshift space galaxy distances include the contribution from peculiar velocities, it is useful to split the separation r into the two components r_p in the plane of the sky, and π along the line-of-sight. The latter variable, π will thus be in this formulation the only one affected by the distortions produced by peculiar motions. These distortions contain important information on cosmological parameters, specifically on the value of $\beta \simeq \Omega_M^{0.6}/b$, where Ω_M is the matter density parameter and b is the so-called *bias* for the specific class of objects being used (Kaiser 1987), on which we shall not discuss here.

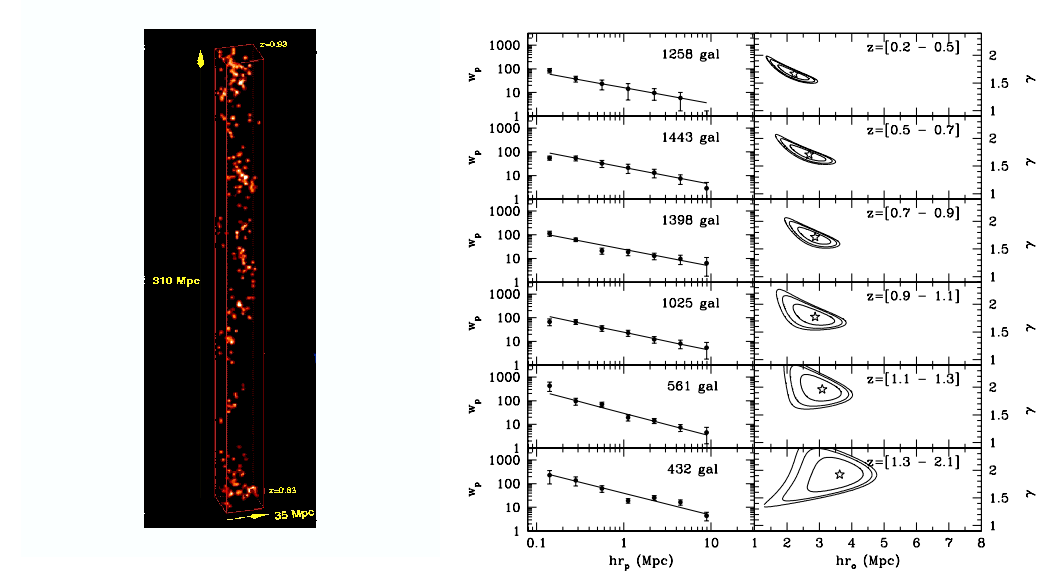

Figure 2: *Left:* Large-scale structure at $z \sim 1$, as seen in a small section of the VVDS light cone. This figure (see Marinoni, this volume) shows the true density field, smoothed on a scale of $2\,h^{-1}$ Mpc and corrected for the survey selection function. *Right:* Measurements of the projected function $w_p(r_p)$ in redshift slices drawn from the full flux-limited VVDS survey, with power-law fits and the corresponding r_0,γ parameters of the real-space correlation function.

$\xi(r_p, \pi)$ is estimated by comparing the observed counts of galaxy pairs at a given separation, with those measured from a random distribution to which we have applied both on the sky and in redshift the same selection function as the observed galaxies. Additionally, pairs are weighted as to take into account systematics effects introduced by the instrumental set-up and observing strategy. In the application to the VVDS data, this procedure has been calibrated and extensively tested using 50 VVDS-Deep mock samples, built from the GalICS simulations (Blaizot et al. 2005). The results have been shown to be robust against the uncertainties in the weighting procedure (Pollo et al. 2005).

The galaxy real-space correlation $\xi(r)$ can thus be recovered, free of distortions, by projecting $\xi(r_p, \pi)$ along the line of sight direction, π (Davis & Peebles 1983)

$$w_p(r_p) \equiv 2 \int_0^\infty \xi(r_p, \pi) d\pi \, . \tag{1}$$

For a power-law spatial correlation function $\xi(r) = (r/r_0)^{-\gamma}$, the integral can be computed analytically, and the projected correlation function can be expressed as

$$w_p(r_p) = r_p \left(\frac{r_0}{r_p}\right)^\gamma \frac{\Gamma\left(\frac{1}{2}\right)\Gamma\left(\frac{\gamma-1}{2}\right)}{\Gamma\left(\frac{\gamma}{2}\right)} \propto r_p^{-\gamma+1} \quad , \tag{2}$$

where Γ is Euler's Gamma function. This model can thus be fit to the observed $w_p(r_p)$ at different redshifts, to estimate the values of r_0 and γ that best describe the global amplitude and slope of the underlying $\xi(r)$. In this way, all the information on $\xi(r)$ at a given redshift is compressed into two numbers. This is useful for a first compact comparison of clustering at different redshifts. However, important information is contained in the detailed shape of $w_p(r_p)$ and $\xi(r)$ (e.g. Guzzo et al. 1991, Zehavi et al. 2004). It is therefore of interest, if the data are sufficient, to go beyond the simple power-law approximation and compare the whole shape of $w_p(r_p)$ at different redshifts (see § 5).

3.2 Observed clustering evolution from the VVDS-Deep flux-limited sample

The right panel of Fig. 2 shows the estimate of $w_p(r_p)$ from the pure flux-limited $I_{AB} < 24$ VVDS-Deep (Le Fevre et al. 2005), within bins at different redshifts, together with the corresponding best-fit values of r_0 and γ. The observed evolution of the correlation lenght r_0 is reproduced more explicitly in the left panel of Fig. 3. The interpretation of this diagram in terms of evolution of structure requires some care. The flux-limited nature of the survey implies that the median intrinsic luminosity of each sub-sample at different redshifts is steadily increasing with redshift. This means that while at $z < 0.5$ we are essentially measuring the clustering of a population of low-luminosity galaxies with typical blue absolute magnitude $M_B \sim -17.5$, in the most distant bin ($z \sim 1.5$), we are sampling only the very luminous $M_B \sim -21$ galaxies. We know that at the current epoch luminous galaxies are more clustered than faint ones (e.g. Norberg et al. 2001). In fact, typical L^* galaxies in the local Universe have a correlation length $r_o \simeq 5\,\mathrm{h}^{-1}\,\mathrm{Mpc}$, to be compared to the value $r_o \simeq 2\,\mathrm{h}^{-1}\,\mathrm{Mpc}$ we measure here in our first redshift bin. Thus, the "evolution" we see in Fig. 2 has little to do with the true evolution of large-scale structure.

This provides us with a first example of how what we actually measure is a combination of true physical evolution and observational selection effects, which are unavoidable in any deep galaxy survey: in particular, the flux limit and the photometric band in which the survey is selected, translate, respectively, into a continuously increasing luminosity limit and a bluer and bluer rest-frame band sampled as a function of redshift. Additionally, the pure evolution of structure is further hidden by the evolution of the relationship between a given population of galaxies (either selected by luminosity, color or morphological type) and the underlying mass distribution. For example, the VVDS has established very clearly that over the redshift range considered, galaxy stellar populations evolve strongly, resulting in a brightening of the galaxy luminosity function of more than a magnitude (Ilbert et al. 2005, Zucca et al. 2006).

So, which galaxies at $z = 0$ should correspond to those we are mesuring at $z = 1$? As far as their clustering is concerned, our ignorance on how the observed galaxy two-point correlation function at a given redshift relates to the true $\xi_\rho(r)$ of the mass density can be parameterized via the *bias parameter* as

$$\xi_g(r, z) = b_L^2(z)\, \xi_\rho(r, z) \ . \tag{3}$$

This expression describes the fact that the galaxy distribution can be in general a "biased" map of the true mass distribution, a concept which has become familiar in cosmology since the 1980's (Kaiser 1984, White et al. 1987). In this simple form, it assumes that the bias is scale-independent, which is probably reasonable above a few Mpc separation. The linear bias b_L will include all or part of the effects mentioned above, depending on how the measured correlation function has been cleaned of the main observational biases. The next section will present the result of trying and circumvent these effects and learn more on how they evolve with redshift.

4 The evolution of galaxy bias

A more general expression for eq. (3) can be written in terms of density contrasts in the galaxy and density fields,

$$\delta_g(\delta, z) = b(\delta, z, R)\delta \ , \tag{4}$$

with $\delta = (\rho - \langle\rho\rangle)/\langle\rho\rangle$, implying that a fluctuation in the galaxy counts can depend on the fluctutation in the mass in a way that is in general non-linear (i.e. depending on the density contrast δ itself), scale-dependent and varying with redshift.

The full function $b(\delta, z, R)$ can be estimated from a redshift survey like the VVDS, by measuring the statistical distribution of galaxy number counts in spheres of a given size R. Once we assume the cosmological model, then the corresponding expected probability distribution function of mass fluctuations $f(\delta)$ can be computed (e.g. Kayo et al. 2001). $b(\delta, z, R)$ can then

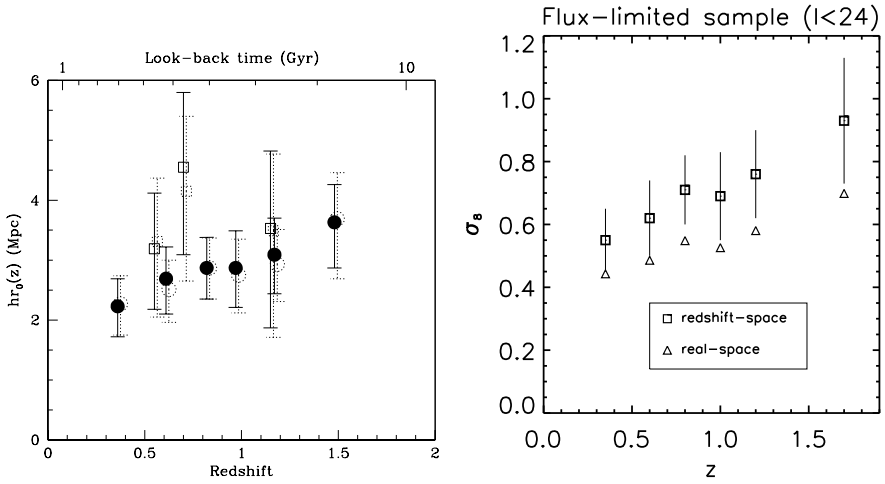

Figure 3: *Left:* Evolution of the correlation length r_0 as a function of redshift using the complete VVDS-Deep flux-limited data. Filled circles are from the F02 field of Fig. 2, while squares are from independent measurements in the CDFS, where VVDS-Deep measured another 1500 redshifts (Le Fevre et al. 2004). Dashed symbols show the effect of fixing $\gamma = 1.8$ in the fit. *Right:* The corresponding trend of the standard deviation in galaxy counts on 8 h^{-1} Mpc scale, in real (triangles) and redshift (squares) space.

be obtained, for a given R and redshift, as the function that maps $f(\delta)$ into the corresponding function $g(\delta_g)$ obtained from galaxy counts. The analysis of the VVDS (Marinoni et al. 2005), shows that the functional form of the bias is in fact generally more complex than the simple linear assumption of eq. 3. Non-linearity between the galaxy fluctuation field δ_g and the matter density field δ is detected (for the first time) at a level of $\sim 10\%$. This result also shows that the linear approximation of the bias, which is useful and intuitive in many contexts, can indeed be used within this level of inaccuracy.

The right panel of Fig. 3 shows the evolution of the standard deviation in the VVDS galaxy counts within spheres of $8\,h^{-1}\,$Mpc, in nearly the same redshift bins used in the left panel for $\xi(r)$. The two figures are essentially equivalent, given the direct relationship between the variance and the two-point correlation function

$$\sigma_R^2 = \frac{1}{2\pi^2}\int_0^\infty P(k)\,W^2(kR)\,k^2\,dk \ . \tag{5}$$

$$P(k) = \int_0^\infty \xi(r)\frac{sin(kr)}{kr}\,r^2\,dr \ , \tag{6}$$

where, W_k is the Fourier transform of the filter over which the observed galaxy distribution is smoothed (in our case, a sphere of radius $R = 8\,h^{-1}\,$Mpc), and $P(k)$ is the power spectrum, the Fourier transform of $\xi(r)$.

In the figure, the squares refer to the values measured in redshift space, while the triangles correspond to the real-space r_0 and γ obtained via the projected function. Note how the variance of the galaxy distribution apparently increases with redshift, following the trend seen for r_0. Again, however, this figure is comparing apples with pears, i.e. very faint galaxies (with small variance) at low redshift, with luminous objects at $z > 1$.

The left panel of Fig. 4, shows instead the result of measuring the second and third moments (standard deviation and skewness) of the galaxy Probability Distribution Function (PDF) on scales of 8 h^{-1} Mpc, as a function of z, using only galaxies brighter than $M_B < -20 + 5\log h$, i.e. in volume-limited sub-samples. This involves measuring the number of galaxies in spheres of 8 h^{-1} Mpc radius and computing the usual statistical quantities. The variance remains now constant over the explored redshift range (while the variance in the matter is expected

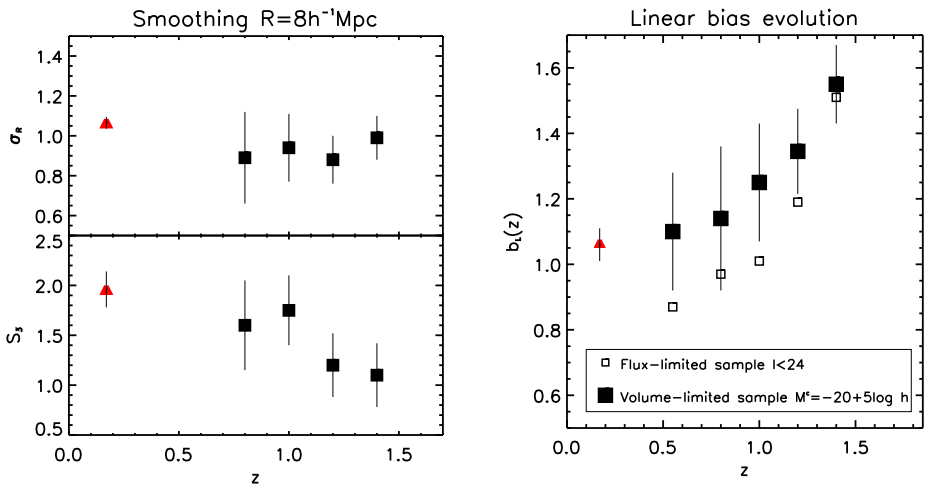

Figure 4: *Left:* Evolution of the standard deviation (top) and skewness (bottom) of the distribution of galaxy counts in spheres of $8\,\mathrm{h}^{-1}\,\mathrm{Mpc}$ size, for a sample with $M_B < -20 + 5\log h$. Comparison to Fig. 3, shows that the observed apparent increase of r_0 and σ_8 for the flux-limited sample in fact results from the combination of the varying luminosity mix (more and more luminous galaxies dominate the redshift bins) with a true increase of the bias value as a function of z. *Right:* The corresponding linear bias evolution (filled squares), compared to that from the full magnitude-limited VVDS (open squares, see text and ref.[33] for details). In all panels, the triangle gives the local values from 2dFGRS[34].

to decrease with redshift as a consequence of gravitational growth). At the same time, the skewness of the PDF becomes smaller as a function of redshift, i.e. going back in time. This is a general expectation of the gravitational instability picture: the growth of fluctuations modifies the initially Gaussian PDF, skewing it towards positive values of δ_g.

In practice, the ratio of the values of σ_8 plotted in Fig. 4 (corrected for redshift-space distortions), to the those expected for the overall dark-matter field in the adopted cosmology, is the linear bias b_L. As we mentioned above, from the VVDS Marinoni et al. (2005) measured the full bias function $b(\delta)$ by inverting the relation between the galaxy and density fields. An unbiased estimator of the linear bias in this case is $b_L^2 = \langle b^2(\delta)\,\delta^2\rangle\,/\,\langle\delta^2\rangle$, which can then be compared to other existing estimates, as we do in the right panel of Fig. 4. Here, the evolution of b_L, computed at different redshifts both for the full flux-limited data set (open squares) and for volume-limited samples with $M_B < -20 + 5\log h$ (filled squares), is shown. Note how the values of the effective bias from the former sample approach asintotically those from the latter, since at increasing redshift it becomes more and more dominated by the same luminous galaxies. This shows explicitly (note the $z \sim 0.1$ 2dFGRS point) how our low-redshift measurements of r_0 from the full VVDS survey refer to a population of faint galaxies apparently anti-biased, i.e. more smoothly distributed than the $\sim L^*$ objects typical of 2dFGRS and SDSS.

Still, also with the volume-limited computation in Fig. 4 we are neglecting the important fact, that also the mean luminosity of galaxies evolves with redshift: galaxies were brighter on average in the past, with a brightening of the characteristic luminosity of the luminosity function in this band, M_B^*, of more than 1 magnitude between $z = 0$ and $z = 1.4$ (Zucca et al. 2006). This means that even with a sample limited to the same absolute magnitude at all redshifts, we are not selecting strictly the same population of objects at different distances/epochs. If we assume this to be a pure luminosity effect (galaxies become brighter with redshift, but conserve their total number in comoving coordinates), this implies that the mass-luminosity ratio in the observed band decreases as a function of redshift. As a consequence, by applying a cut at constant luminosity $M_B < -20$, we are including at increasing redshifts galaxies of smaller and smaller mass. Thus, had one used an evolving limit, e.g. by selecting galaxies brighter than a

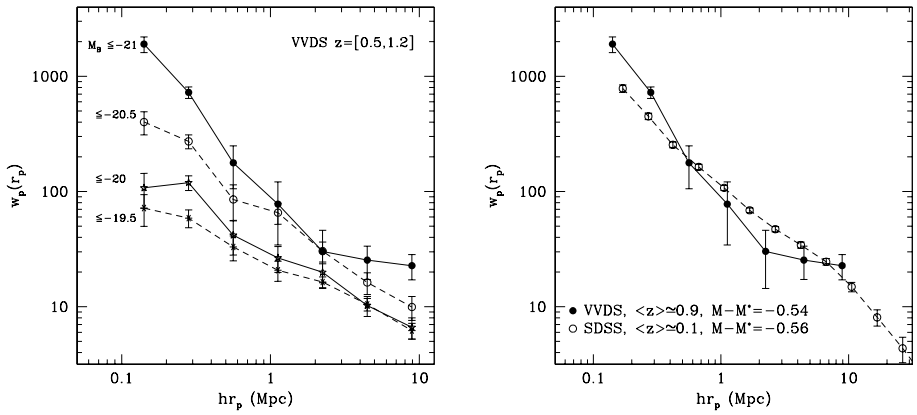

Figure 5: *Left:* Projected correlation function $w_p(r_p)$ from four high-redshift volume-limited sub-samples of the VVDS with increasing luminosity. *Right:* Comparison of the SDSS and VVDS measurements for samples with comparable luminosity (relative to L^*) respectively at $z \simeq 0.1$ and $z \simeq 0.9$.

fixed $L_{lim}(z)/L^*(z)$ (i.e. a constant $M_{lim}(z) - M^*(z)$), the resulting "true" (i.e. mass-related) bias evolution would be even steeper. We have used this approach to study the dependence of clustering on absolute luminosity at $z \sim 1$ in the VVDS and compare it to local results, as discussed in the next section.

5 Clustering of galaxies with different luminosity at $z = 1$

At the current epoch, luminous galaxies are observed to be more clustered than faint ones (e.g.Norberg et al. 2001 and references therein), with this difference becoming more significant above the characteristic luminosity L^*. This effect is in general agreement with the predictions from hierarchical models (e.g. Benson et al. 2001), in which bright galaxies are expected to form in more massive dark matter halos, which are typically more strongly clustered than the overall distribution of dark matter (Kaiser 1984, Mo & White 1996). In this scenario, these differences should be enhanced at high redshifts, where galaxy formation is expected to be more and more confined to the highest peaks of the density field.

We have addressed this issue with the VVDS, by measuring the correlation functions $\xi(r_p, \pi)$ and $w_p(r_p)$ for a series of sub-samples with increasing median luminosity M_B comprised between -19.7 and -21.3 and covering the redshift range [0.5-1.2] (median redshift $z \simeq 0.9$) (Pollo et al. 2006). The left panel of Fig. 5 shows the projected function for the four brightest volume-limited high-redshift sub-samples of the VVDS. The right panel instead makes a direct comparison of the shape of $w_p(r_p)$ for galaxies with the same relative luminosity (~ 0.5 magnitudes brighter than M_B^*) in the SDSS at $z \sim 0.1$ and in the VVDS at $z \sim 0.9$. This trick of expressing the typical luminosity of a sample relatively to the characteristic luminosity L^* at the same epoch is an attempt to factor out the overall luminosity evolution, thus hopefully comparing galaxies of similar mass at different redshifts. Two main effects are evident from these figures. On one side, the clustering amplitude does depend on luminosity also at redshifts of the order of unity. Additionally, however, we observe a steepening of the small-scale part of $w_p(r_p)$ for highly-luminous galaxies, significantly stronger than in local SDSS samples (Zehavi et al. 2005).

This effect can be seen even more explicitly in Fig. 6, where we compare our measurements of r_0 and γ from the VVDS samples to the local values from 2dFGRS (Norberg et al. 2001) and SDSS (Zehavi et al. 2005): galaxies fainter than M_B^* at high redshift are significantly less clustered than their counterparts in the present-day Universe (left panel). At the same time, the

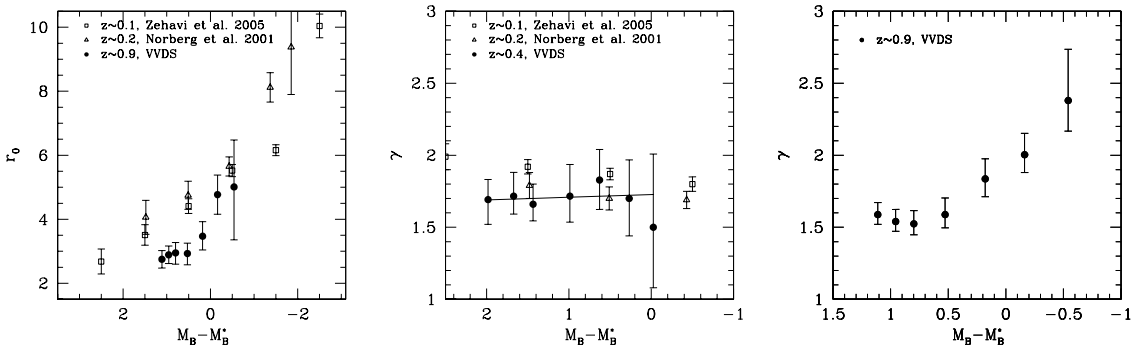

Figure 6: *Left:* The dependence of the clustering length r_0 on galaxy luminosity from 2dFGRS and SDSS compared to the VVDS measurements at $z \sim 0.9$. *Center:* Values of the slope of $\xi(r)$, γ, as a function of luminosity at low redshift . *Right:* The same, but at $z \sim 0.9$. Note the dramatic steepening of $\xi(r)$ at increasing luminosities in this redshift range.

clustering strength of galaxies brighter than M_B^* is comparable to that observed locally with a correlation length up to $r_0 = 4.77 \pm 0.61$ h^{-1} Mpc. We therefore observe that at redshift $z \simeq 0.9$, as luminosity increases above L^*, the clustering length suddenly rises to values comparable to those observed locally for galaxies with similar $M_B - M_B^*$. It is the slope γ, however, that shows the most dramatic difference when comparing the $z \sim 0$ and $z \sim 1$ results, and from Fig. 5 we see that this change is mostly confined to scales $r_p < 2\,\mathrm{h}^{-1}\,\mathrm{Mpc}$. A parallel, analogous work on the DEEP2 data (Coil et al. 2006) finds a similar result, with slightly less pronounced steepening. Even more interestingly, Ouchi et al. (2005) observe the same phenomenon studying the clustering of Lyman-break selected galaxies at $z \sim 4$. In this analysis, they also find that it is the small-scale part of the correlation function which is the most sensitive to the mean luminosity of the sample, steepening for more luminous galaxies as in the case of the VVDS at $z \sim 1$.

Although with a much less evident steepening (note that the slope in the central panel of Fig 6 is measured between 0.1 and 10 h^{-1} Mpc, thus weakening any small-scale effect), the existence of a feature in $\xi(r)$ on scales $\sim 1 - 3$ h^{-1} Mpc is in fact a well-established observation also for luminous galaxies in the local Universe. First evidences go back to analyses of the pioneering redshift surveys of 1980's, as the CfA and Perseus-Pisces surveys (Dekel & Aarseth 1984; Guzzo et al. 1991), where quite naturally this feature was interpreted as marking the transition scale between the linear regime of clustering on large scales and fully nonlinear structures on small scales. This picture was found to be consistent with both numerical (Branchini et al. 1994) and analytical (Peacock 1997) results on the non-linear evolution of phenomenological scale-free or CDM-like power spectra. The same effect was also particularly evident in the power spectrum obtained from deprojection of the APM angular correlation function (Baugh & Efstathiou 1993, see also Guzzo 1997 and Gaztañaga & Juszkiewicz 2001), and in the reconstructed shape of the general galaxy power spectrum (Peacock & Dodds 1994).

The reality of this feature in the galaxy correlation function has been confirmed to high accuracy in more recent times by the SDSS data (Zehavi et al. 2004) and interpreted in the context of *halo occupation distribution (HOD)* models. In these models, a statistically motivated recipe to describe galaxy formation determines the halo occupation distribution, specifying the probability $P(N|M)$ that a dark matter halo of virial mass M contains N galaxies of a given type. This term (known as the *one-halo component* of the correlation function) governs the behaviour of galaxy correlations on small (< 2 h^{-1} Mpc) scales (i.e. where $w_p(r_p)$ steepens), while at larger separations galaxy correlations are described by the quasi-linear clustering of the halos (the *two-halo component*), with essentially no dependence on the more complex physics of

the sub-dominant baryonic component (see Cooray & Sheth 2002 for a comprehensive review). The modern HOD scenario, therefore, confirms the interpretation of the small-scale steepening of galaxy correlations as the transition to fully non-linear clustering, as speculated in Guzzo et al. (1991), but specifying it as the scale below which correlations are dominated by pairs of galaxies belonging to the same dark-matter halo.

HOD models are found to provide a better description of the non-linear clustering of galaxies with respect to analytical scaling formulae (as e.g. the remarkable one by Hamilton et al. 1991), used in earlier times to predict the observed non-linear shape of the galaxy power spectrum or correlation function (see e.g. Smith et al. 2003). Still, the number of free parameters that need to be constrained by comparison to observed properties (as e.g. the dependence of clustering on galaxy luminosity or color), make the overall technique not fully satisfactory. Recently, there have been interesting attempts to go beyond this substantially statistical description of what happens to galaxies on sub-halo scales (Conroy et al. 2006; Wang et al. 2006). These works try to improve the definition of galaxies within dark-matter halos identified in N-body simulations, in particular by accounting for objects whose dark-matter halos are destroyed by tidal effects, but that still survive in their baryonic component. Conroy et al. (2006) specifically study the dependence of the shape of the two-point correlation function on luminosity at different redshifts. Remarkably, they correctly reproduce the small-scale upturn of the correlation function in luminosity-selected samples and also show (as we have found from our comparison of the VVDS and SDSS data), that this deviation is stronger at higher redshifts and for more luminous objects.

Along these lines, work is in progress to perform accurate comparisons of VVDS to mock galaxy surveys from the Millennium Simulation.

6 The clustering of different galaxy types up to $z \sim 1.5$

It is quite plausible that the relationship between galaxies and their parent dark-matter halos depend on the galaxy type or, better, that the physical morphological properties of galaxies depend in some way on the properties of the hosting halo, as e.g. its mass. In fact, it is a well-established observational fact in the local Universe that red galaxies are more clustered than blue galaxies, which at least at $z = 0$ is equivalent to say that early-type (elliptical and S0's) galaxies are more strongly packed among themselves than late-type (spiral and irregular) ones (e.g. Guzzo et al. 1997 and references therein). In the now familiar bias jargon introduced in the previous sections, we may rephrase this by saying that red galaxies are a *more biased* population than blue galaxies, and thus a less faithful tracer of the true mass distribution. Indeed, elliptical and S0 galaxies are the preferred population of rich galaxy clusters, giving rise to the well known morphology-density relation (e.g. Dressler 1980).

It is thus natural to ask: is this difference already established at redshifts $z \sim 1$? And is the way this difference evolves with redshifts telling us anything about the way galaxies in general trace the underlying structure evolution? One possibility, for example, is that old massive elliptical galaxies are simply passively evolving within this redshift range (e.g. Cimatti et al. 2006), and thus their clustering should follow almost passively the growth of structure. The alternative scenario is that of a significant merging activity since $z \sim 1$ to today (e.g. Bell et al. 2004), that should manifest itself in a different evolution of the clustering of this population.

We have addressed this issue with the VVDS data, and the results are presented in the recent paper by Meneux et al. (2006). Galaxies have been split into four spectral classes, according to a best-fitting template procedure to their multi-band photometry, as discussed in detail in Zucca et al. (2006). The left panel of Fig. 7 presents the evolution of the correlation lenght r_o between $z \sim 0.3$ and $z \sim 1.5$, for early- and late-type galaxies separately. The main result from this plot is that at least out to $z \sim 1.2$ red galaxies remain more clustered than blue galaxies.

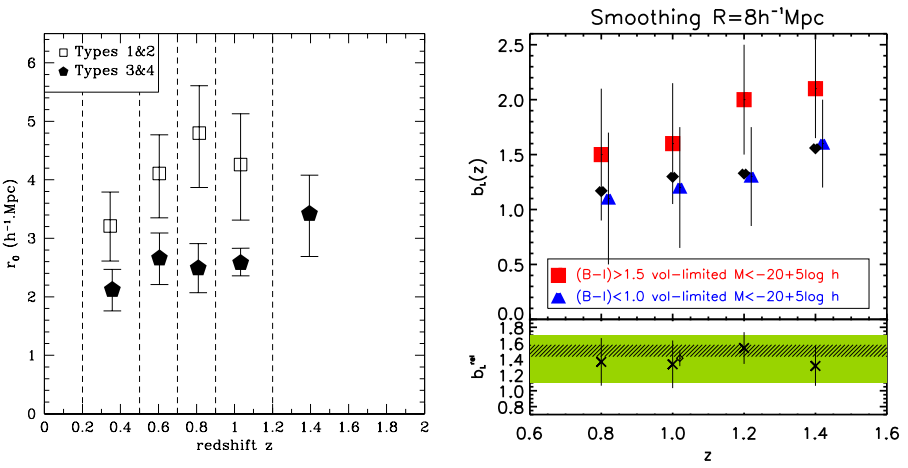

Figure 7: *Left:* Evolution of r_0 for red (open symbols, spectral types $1+2$) and blue (filled symbols, types $3+4$) galaxies from the whole VVDS (Meneux et al. 2006). *Right:* The linear bias of red (squares) and blue (triangles) galaxies with respect to dark matter, computed as discussed in the text, for samples with $M_B < -20 + 5\log h$. Small filled lozenges show the value for all types, corresponding to the right panel of Fig. 4. The bottom panel gives the relative bias of the two classes, that remains constant over this range.

Being obtained from the full flux-limited survey, this plot includes the same luminosity effect discussed in section 3.2, i.e. it compares low-luminosity objects at $z \sim 0.3$ with the most luminous galaxies at $z > 1$. In fact, we know from local samples (e.g. Guzzo et al. 1997) that bright $M_B \sim M_B^* \simeq -19.5$ galaxies at $z \sim 0$ show $r_o \simeq 8\,\mathrm{h}^{-1}$ Mpc and $r_o \simeq 5\,\mathrm{h}^{-1}$ Mpc for early- and late-types respectively. The plot shown in the right panel of Fig. 7 Marinoni et al. 2005), again tries to overcome this problem, at the expense of reducing the sample significantly by selecting – at any redshift – only galaxies brighter than a fixed intrinsic luminosity. Here the relative strength of clustering of early and late spectral types is expressed in terms of their linear bias, computed as in Fig. 4 (see Marinoni et al. 2005 for details). The net result is that out to $z \sim 1.5$ the relative bias between red and blue galaxies remains practically constant, as shown explicitly in the bottom part of the figure. This seems apparently to contraddict the recent measurement from the same VVDS data of a clear evolution of the color-density relation. As discussed in detail in the recent paper by Cucciati et al. (2006), the VVDS data show that the color-density relation weakens significantly above $z \sim 1$, suggesting that star-forming galaxies start to populate more and more the high-density regions.

The difference with Fig. 7 might perhaps be just the consequence of different sensitivity of the first and second moments (density and variance) to changes in the global environment: finding blue or red galaxies in high-density regions at $z \sim 1.4$ becomes equally probable, but still the number of small-scale pairs is larger for red objects. On the other hand, the higher-redshift point for red galaxies in the right panel of Fig. 7 is also affected by small statistics (and in fact there is no equivalent point at $z = 1.4$ in the left panel, where a differential quantity – the correlation function – is used). Additional work which is in progress using Spitzer photometry from the Swire survey (Lonsdale et al. 2003), is in fact indicating a similar clustering level at $z \sim 1.5$ for luminous, blue-selected star-forming galaxies and NIR-selected, massive objects (de la Torre et al. 2007), thus in agreement with the trend indicated by the color-density relation. This is one of several investigations on the relationship between large-scale structure and galaxy properties, that are ongoing with the VVDS data. Further boost to these researches will come from the completion of the redshift measurements for the $\sim 33,000$ spectra collected over the *VVDS-Wide* fields (Garilli et al. 2007) and the combined use of the *VVDS-Deep* spectroscopic sample with the high-quality photometric redshifts obtained in the surrounding area using the

additional CFHT-LS photometry (Ilbert et al. 2006). In addition to extending and improving the results obtained from *VVDS-Deep*, cosmological tests requiring sampling large volumes and scales $\gg 10$ h^{-1} Mpc will become feasible for the first time at $z \sim 1$ thanks to the large area coverage provided by the *VVDS-Wide* data. These include, for example, the measurement of $\beta \simeq \Omega_M^{0.6}/b$ from the the distortions of $\xi(r_p, \pi)$. Realistic simulations show that with the planned full *Wide* survey ($\sim 100,000$ redshifts over ~ 10 square degrees), β can be measured at $z \sim 1$ to an accuracy of 10% (Pierleoni et al., 2007), thus providing an estimate of the mean matter density when the Universe was about half its current age.

Acknowledgments

LG thanks the organizers of the Moriond 2006 workshop for kindly inviting him to present this review and J. Blaizot, G. De Lucia, G. Kauffmann and S. White for stimulating discussions on galaxy clustering and HOD models. ESO and the Max-Planck Insitut für Astrophysik are also gratefully acknowledged for their hospitality and for providing a stimulating atmosphere during the completion of this paper.

References

1. Adelman-McCarthy, J.K., et al., ApJS, **162**, 38 (2006)
2. Baugh, C.M., Efsthathiou, G., MNRAS **265**, 145 (1993)
3. Bell, E., et al., ApJ **608**, 752 (2004)
4. Benson, A. J., Cole, S., Frenk, C. S., Baugh, C.M., Lacey, C.G., MNRAS **327**, 1041 (2001)
5. Blaizot, J., et al., MNRAS **360**, 159 (2005)
6. Borgani S. & Guzzo L., Nature **409**, 39 (2001)
7. Borgani, S., et al., ApJ **561**, 13 (2001)
8. Branchini, E., Guzzo, L., Valdarnini, R., ApJ **424**, L5 (1994)
9. Broadhurst, T.J., Ellis, R.S., Shanks, T., MNRAS **235**, 827 (1988)
10. Cimatti, A., Daddi, E., Renzini, A., AA **453**, L29 (2006)
11. Coil, A.L., et al. ApJ **644**, 671 (2006)
12. Cole, S., et al., MNRAS **362**, 505 (2005)
13. Colless, M., et al., MNRAS **328**, 1039 (2001)
14. Conroy, C., Wechsler, R., Kravtsov, A.V., ApJ 647, **201** (2006)
15. Cooray, A. & Sheth, R., Phys. Rept., **372**, 1 (2002)
16. Croton, D.J., et al., MNRAS **352**, 1232 (2004)
17. Cucciati, O., Iovino, A., Marinoni, C., et al. (VVDS Consortium), AA **458**, 39 (2006)
18. Davis, M., Peebles, P.J.E., ApJ **267**, 456 (1983)
19. Dekel, A., Aarseth, S., ApJ **283**, 1 (1984)
20. de la Torre, S., et al. (VVDS Consortium), AA, submitted
21. Dressler, A., ApJ **236**, 351 (1980)
22. Eisenstein, D., et al., ApJ **633**, 560 (2005)
23. Garilli, B., et al. (VVDS Consortium), in preparation (2007)
24. Gaztañaga, E., Juszkiewicz, R., ApJ **558**, L1 (2001)
25. Guzzo, L., et al., ApJ **382**, L5 (1991)
26. Guzzo, L., NewA, **2**, 517 (1997)
27. Guzzo, L., et al., ApJ **489**, 37 (1997)
28. Hamilton, A.J.S., Kumar, P., Lu, E., Matthews, A., ApJ **374**, L1 (1991)
29. Ilbert, O., Tresse, L., Zucca, E., et al. (VVDS Consortium), AA **439**, 863 (2005)
30. Ilbert, O., Arnouts, S., McCracken, H.J., AA **457**, 841 (2006)
31. Jenkins, A., et al., MNRAS **321**, 372
32. Kaiser, N., MNRAS **227**, 1 (1987)
33. Kaiser, N., ApJ **284**, L9 (1984)
34. Kauffmann, G., et al., MNNRAS **307**, 529 (1999)
35. Kayo, I., Taruya, A., Suto, Y., ApJ **561**, 22 (2001)

36. Lacey, C., Cole, S., MNRAS **262**, 627 (1993)
37. Le Fèvre, O., et al., ApJ **461**, 534 (1996)
38. Lonsdale, C.J., Smith, H.E., Rowan-Robinson, M.J., et al., PASP **115**, 897 (2003)
39. Le Fèvre, O., Vettolani, G., Paltani, S., et al. (VVDS Consortium), AA **328**, 1043 (2004)
40. Le Fèvre, O., Vettolani, P., Garilli, B., et al. (VVDS Consortium), AA **439**, 845 (2005)
41. Le Fèvre, O., Guzzo, L., Meneux., B. et al. (VVDS Consortium), AA **439**, 877 (2005)
42. Lilly, S., et al. (the zCOSMOS Team), ApJS COSMOS Special Issue, (2007) in press
43. Marinoni, C., Le Fèvre, O., Meneux, B. et al. (VVDS Consortium), AA **442**, 801 (2005)
44. Meneux, B., Le Fèvre, O., Guzzo, L., et al. (VVDS Consortium), AA **452**, 387 (2006)
45. Mo, H.J., & White, S.D.M., MNRAS **282**, 347 (1996)
46. Norberg, P., Baugh, C.M., Hawkins, E. et al, MNRAS **328**, 64 (2001)
47. Ouchi, M., ApJ **635**, L117 (2005)
48. Peacock, J.A., MNRAS **284**, 885 (1997)
49. Peacock, J.A., Dodds, S.J., MNRAS **267**, 1020 (1994)
50. Pierleoni, M., et al., in preparation (2007)
51. Pollo, A., Meneux, A. Guzzo, L., et al. (VVDS Consortium), AA **439**, 887 (2005)
52. Pollo, A., Guzzo, L., Le Fèvre, O., et al. (VVDS Consortium), AA **451**, 409 (2006)
53. Press, W. H., & Schechter, P. ApJ **187**, 425 (1974)
54. Rosati, P., Borgani, S., & Norman, C., ARAA **40**, 139 (2002)
55. Sheth, R.K., & Tormen, G., MNRAS **308**, 119 (1999)
56. Smith, R.E., et al. MNRAS **341**, 1311 (2003)
57. Somerville, R.S., Primack, J.R., MNRAS **310**, 1087 (1999)
58. Wang, L., Cheng, L., Kauffmann, G., & De Lucia, G., MNRAS **371**, 537 (2006)
59. White, S.D.M., Frenk, C.S., Davis, M. & Efstathiou, G., ApJ **313**, 505 (1987)
60. Yee, H.K.C., et al., ApJS, **129**, 475 (2000)
61. Zehavi, I., et al., ApJ **608**, 16 (2004)
62. Zehavi, I., Zheng, Z., Weinberg, D.H. et al., ApJ **630**, 1 (2005)
63. Zucca, E., Ilbert, O., Bardelli, S., et al. (VVDS Consortium), AA **455**, 87 (2006)